Journal homepage: http://gwse.iheg.org.cn

Research Article

Natural brown coal as an adsorbent for manganese removal from groundwater: A mechanistic and operational evaluation

Obiri-Nyarko F[1*], Darko DA[2], Quansah JO[3], Asare SV[1], Karikari AY[3]

[1] *Groundwater and Geoscience Division, CSIR-Water Research Institute, P.O. Box M32, Accra, Ghana.*
[2] *Institute for Environment and Sanitation Studies, College of Basic and Applied Sciences, University of Ghana, Legon, Accra – Ghana.*
[3] *Environmental Chemistry and Sanitation Engineering Division, CSIR-Water Research Institute, P.O. Box M32, Accra, Ghana.*

Abstract: This study investigates the potential of natural Brown Coal (BC) as a sustainable, cost-effective adsorbent for the removal of manganese (Mn^{2+}) from contaminated groundwater. A series of batch adsorption experiments was conducted to assess the influence of key operational parameters—such as solution pH, initial Mn^{2+} concentration, BC dosage, temperature, and the presence of competing ions—on Mn^{2+} removal efficiency. The environmental compatibility and regeneration potential of BC were also evaluated to determine its practical viability for repeated use. To better understand the adsorption behaviour, equilibrium and kinetic data were analysed using established isotherm and kinetic models, while thermodynamic parameters were computed to assess the spontaneity and thermal characteristics of the adsorption process. Furthermore, geochemical modelling and comprehensive BC characterization—including surface morphology, mineralogical and elemental composition, and functional group analysis—were performed to elucidate Mn^{2+} speciation under varying environmental conditions and to uncover the underlying adsorption mechanisms. Results showed that Mn^{2+} removal efficiency increased with higher pH, temperature, and BC dosage, but declined at elevated initial Mn^{2+} concentrations due to active site saturation. The process was spontaneous and endothermic, with the Langmuir isotherm model (R^2 = 0.994) and pseudo-second-order kinetic model (R^2 = 0.996) providing the best fit to experimental data. Mechanistic analysis indicated that chemisorption, primarily through ion exchange and inner-sphere complexation, was the dominant mode of Mn^{2+} uptake. The presence of competing cations, especially Fe^{3+} and Cu^{2+}, significantly hindered Mn^{2+} removal due to preferential binding. Importantly, BC exhibited strong reusability, maintaining over 80% removal efficiency across four adsorption–desorption cycles without evidence of secondary pollutants. These findings demonstrate the potential of natural BC as an efficient, reusable, and environmentally benign material for treating manganese-contaminated groundwater.

Keywords: Sorption; Surface complexation; Ion exchange; Geochemical modelling; Heavy metals; Secondary pollution

Received: 25 Sep 2024/ Accepted: 21 Aug 2025/ Published: 10 Oct 2025

Introduction

In Ghana, groundwater is a vital source of drinking water, particularly in rural communities and small towns, where it supplies over 95% of domestic water needs (Debrah et al. 2024; Biney et al. 2024). However, numerous studies have reported high concentrations of Heavy Metals (HMs), including Manganese (Mn) (Zhang et al. 2025; Chen et al. 2024), in groundwater across various regions of the country (Biney et al. 2024; Tabi et al. 2024). Manganese is widely distributed in terrestrial environments and typically occurs in the divalent form Mn^{2+} under acidic and anaerobic conditions (Çalışır et al. 2024).

Mn plays an essential role in many biological

*Corresponding author: Obiri-Nyarko F, *E-mail address*: Fobiri-nyarko@csir.org.gh

DOI: 10.26599/JGSE.2025.9280060

Obiri-Nyarko F, Darko DA, Quansah JO, et al. 2025. Natural brown coal as an adsorbent for manganese removal from groundwater: A mechanistic and operational evaluation. Journal of Groundwater Science and Engineering, 13(4): 371-385.

processes across living organisms, including humans. It acts as a cofactor for enzymes, such as arginase, which is involved in the urea cycle, and functions as an antioxidant protecting cells from damage caused by reactive oxygen species (Caldwell et al. 2018). High levels of Mn, particularly in drinking water, on the other hand, poses significant health risks. Prolonged Mn exposure can lead to the accumulation of Mn in the central nervous system, with potential neurotoxic effects (McKinley et al. 2019). In children, ingestion of Mn-contaminated water has been linked to developmental disorders, such as cognitive impairment and behavioural abnormalities, especially when concentrations exceed the World Health Organization (WHO) guideline value of 0.4 mg/L (Jakariya et al. 2024). In adults, high Mn exposure has been associated with a variety of neurological and psychological disorders, including depression, hypersomnia, and Parkinsonism (Sönmez and Hocaoğlu, 2023). Furthermore, high levels of Mn^{2+} in drinking water can lead to serious aesthetic and operational challenges, including unpleasant taste, discolouration, and pipeline clogging due to the oxidation of Mn^{2+} to insoluble Mn^{3+} and Mn^{4+} oxides, which precipitate and accumulate within water distribution systems (Galangashi et al. 2021). Given the dual challenges posed by Mn contamination, both from public health and operational issues, it is critical to either protect water sources from Mn pollution or develop effective and affordable treatment techniques to remove Mn from groundwater.

In the field of water treatment, several methods, including electrocoagulation, membrane separation, adsorption, catalytic oxidation, and chemical precipitation, have been explored at the laboratory scale to remove Mn^{2+} from water (Neculita and Rosa, 2019; Virolainen et al. 2021; Jiang et al. 2023; Panagopoulos and Michailidis, 2025). While these techniques have demonstrated promising removal efficiencies, many face significant practical limitations, such as high energy consumption, high costs of implementation and maintenance, and waste disposal issues. For instance, membrane-based approaches require pre-treatment steps and are often hindered by membrane fouling due to pore blockage or cake deposition, which reduces their long-term viability (Panagopoulos and Michailidis, 2025). Similarly, catalytic oxidation techniques that rely on strong oxidants such as $KMnO_4$, O_3, ClO_2, and NaClO of Mn also increases treatment costs and poses environmental risks due to residual chemicals that may contaminate the environment (Jiang et al. 2023). These drawbacks present significant challenges to the delivery of safe and cost-effective potable water. Adsorption, on the other hand, has become a more feasible option for purifying contaminated water due to its high operability. The performance of adsorption processes is influenced by multiple factors, including the physicochemical characteristics of the adsorbent and the pollutants, the nature of their interactions, and the quality and composition of the water matrix (Chen et al. 2022). For manganese, removal efficiency depends on key factors such as solution pH, adsorbent dosage, temperature, and initial Mn^{2+} concentration (Kobielska et al. 2018). Therefore, optimizing these conditions is critical for the effective design and implementation of adsorption systems. However, conducting extensive laboratory experiments to identify optimal conditions can be costly and time-consuming. To address this, geochemical simulation tools, such as PHREEQC and Visual MINTEQ, have been increasingly employed to complement experimental investigations (Quansah et al. 2024). These specialized tools are capable of simulating a wide range of adsorption processes under diverse environmental conditions, offering insights into solute speciation, transport mechanisms, and removal efficiencies, while also reducing experimental burden and guiding the development of scalable treatment strategies.

The growing emphasis on sustainability and cost efficiency has spurred interest in using low-cost, natural, and locally available adsorbents as alternatives to more expensive materials like activated carbon. These natural materials offer environmentally friendly and economically viable solutions for mitigating water pollution, particularly in resource-limited settings. Their widespread availability, low cost, and minimal processing requirements make them particularly attractive for large-scale applications in developing regions, where access to advanced treatment technologies is often constrained (Rudi et al. 2020). Brown Coal (BC), also known as lignite, is a naturally occurring material formed from the gradual diagenesis of peat and other mineral matter under prolonged heat and pressure. BC is recognized for its high cation exchange capacity and selective adsorption of metal ions (Tu et al. 2019; Sun et al. 2023; Quansah et al. 2024), a characteristic attributed to the presence of functional groups and mineral phases within the BC. However, the adsorptive performance of BC can vary significantly depending on its source and composition, necessitating sample-specific evaluation prior to any practical application (Quansah et al. 2024). A previous

study by Quansah et al. (2024) demonstrated that BC is effective in removing Fe from contaminated groundwater. Building on this work, the present study explores the potential of BC to remove Mn^{2+} from polluted groundwater. Laboratory experiments were conducted to examine the effects of key operational parameters, including pH, initial Mn^{2+} concentration, BC dosage, temperature, and the presence of competing ions on adsorption efficiency. In addition, BC was characterized to determine its physicochemical properties, and geochemical simulations using Visual MINTEQ were performed to gain further insight into Mn speciation and the associated adsorption mechanisms. The study also assessed the reusability and environmental safety of BC, providing a holistic evaluation of its suitability as a sustainable and effective material for groundwater treatment.

1 Materials and methods

1.1 Aqueous solution preparation and adsorbent characterization

A 10 mg/L manganese (Mn^{2+}) solution was prepared by diluting a 1,000 mg/L stock solution (obtained from Wagtech Ghana Ltd.) in a 1,000 mL volumetric flask. All the chemical solutions used in this study were prepared using reagent-grade chemicals and deionized water to ensure analytical precision. The BC used as the adsorbent was obtained from a local depot in central Accra, Ghana. It was air-dried and sieved through a 200-mesh standard soil sieve (75 μm) to eliminate impurities and achieve a uniform particle size distribution. To evaluate the surface charge properties of BC, the point of zero charge (pH_{pzc}) was determined. Surface area and pore volume were evaluated using nitrogen adsorption-desorption analysis conducted with a Micromeritics ASAP 2460 instrument at 77 K, applying the Brunauer-Emmett-Teller (BET) method. Functional groups present on the BC surface were identified through Fourier Transform Infrared (FTIR) spectroscopy using a Brucker Equinox 55 spectrometer. To analyse the elemental composition and surface morphology, Scanning Electron Microscopy (SEM) coupled with Energy Dispersive X-ray (EDX) Spectroscopy (Zeiss EVO MA 15, Germany) was employed. The mineralogical composition of the BC was determined using a Bruker D8 Advanced X-ray Diffractometer (XRD) equipped with Cu Kα radiation. In addition, proximate analysis was performed using a Carbolite Eurotherm furnace (OAF 2216e) to determine the moisture, fixed carbon, volatile matter and ash content of the BC.

1.2 Adsorption studies

To evaluate the equilibrium adsorption capacity of the BC, isotherm experiments were conducted using Mn^{2+} solutions with concentrations ranging from 1 mg/L to 50 mg/L. Adsorption kinetics were studied by varying the contact time from 30 minutes to 420 minutes, with samples collected at 30-minute intervals to determine residual Mn^{2+} concentrations. The influence of solution pH on Mn^{2+} removal efficiency was assessed by adjusting the initial solution pH between 2 and 12 using 0.1 M HCl or NaOH. To evaluate the thermodynamic behaviour of the adsorption process, the solution temperatures were varied from 25°C to 120°C. The reusability of BC was investigated through adsorption and desorption cycles using 0.1 M HCl as the desorbing agent. Additionally, the impact of competing ions, including Ca^{2+}, Na^{+}, K^{+}, Cu^{2+}, Zn^{2+}, and Fe^{3+}, on Mn^{2+} removal was studied in binary systems. Further experiments were conducted to determine the influence of initial Mn^{2+} concentrations (ranging from 1 mg/L to 150 mg/L) and BC dosages (from 0.2 g to 5 g) on adsorption efficiency. To examine the environmental safety of BC, ion leaching into the solution during the experiments was also monitored. All experiments were conducted in amber glass bottles placed on an orbital shaker (SHEL LAB S16/S16R) operating at 150 rpm. After each run, BC was separated from the solution using a vacuum pump (FB 70155, Fisherbrand). Mn^{2+} concentrations were measured using an atomic absorption spectrophotometer (AAS, Agilent Technologies 240 FS 200 Series), while pH was monitored using a HACH pH meter. Each experiment was performed in duplicate, with average values used for analysis. The amount of Mn^{2+} adsorbed at equilibrium and specific time intervals was calculated using Equations (1) and (2), respectively (Tu et al. 2019; Quansah et al. 2024).

$$q_e = v\left(\frac{C_0 - C_e}{m}\right) \quad (1)$$

$$q_t = v\left(\frac{C_0 - C_t}{m}\right) \quad (2)$$

Where: q_e and q_t are the amounts of Mn^{2+} adsorbed (mg/g) at equilibrium and time (t), respectively; C_0, C_e and C_t (mg/L) are the initial, equilibrium and time-specific Mn^{2+} concentrations, respectively; m is mass of BC used (g); and v is the

solution volume (L).

To model adsorption kinetics, the Pseudo-First-Order (PFO) (Eq. 3), Pseudo-Second-Order (PSO) (Eq. 4) and Intra-Particle Diffusion (IPD) (Eq. 5) models were applied (Wang and Guo, 2020; Quansah et al. 2024).

$$q_t = q_e\left[1-\exp\left(-k_1 t\right)\right] \tag{3}$$

$$\frac{1}{q_e - q_t} = \frac{1}{q_e} + k_2 t \tag{4}$$

$$q_t = k_p t^{1/2} + C_i \tag{5}$$

Where: q_t denotes the quantity of Mn^{2+} adsorbed at time t per unit mass of BC (mg/g), q_e represents the adsorbed Mn per unit mass of BC at equilibrium (mg/g), k_1 (1/h) and k_2 (g/mg/h) represent rate constants for the pseudo-first-order and pseudo-second-order kinetic models. k_p which denotes the intraparticle diffusion rate constant of stage i (mg/g $h^{1/2}$), was derived from the slope of the linear relationship between q_t and $t^{1/2}$. C_i represents the intercept of stage i, and it provides an approximation of the thickness of the boundary layer, where a larger intercept implies a more significant boundary layer effect.

The sorption isotherms were analysed using the Langmuir (Eq. 6) and Freundlich (Eq. 7) models (Fseha et al. 2022; Obiri-Nyarko et al. 2022). The Langmuir isotherm is predicated on monolayer adsorption and presupposes adsorption onto a uniform surface (Zhao and Naeth, 2024). Freundlich isotherm, on the other hand, posits that the adsorption takes place on a heterogeneous surface, and involves interactions among the adsorbed molecules. Adsorption tends to be favourable when the Freundlich isotherm constant n falls within the range of 1 to 10. Large values of n (corresponding to small values of $1/n$) suggest a more robust interaction between the adsorbate and the adsorbent, while a value of 1/n equal to unity signifies linear adsorption, resulting in uniform adsorption energies across all sites (Kwakye-Awuah et al. 2019). A value of 1/n less than 1 signifies a typical Langmuir isotherm, while 1/n greater than 1 denotes cooperative adsorption (Zhao and Naeth, 2024).

$$q_e = \frac{Q_m K_L C_e}{1+K_L C_e} \tag{6}$$

$$q_e = K_F C_e^{\,1/n} \tag{7}$$

Where: K_L (L/mg) is the Langmuir adsorption constant associated with the binding energy; Q_m (mg/g) is the Langmuir maximum adsorption capacity; K_F (L/g) denotes the distribution coefficient; and n is the Freundlich constant.

The thermodynamic parameters, enthalpy change $\Delta H°$, Gibbs free energy change $\Delta G°$, and entropy change ΔS° were calculated using Eqs. (8) – (11) (Quansah et al. 2024):

$$\Delta G^\circ = \Delta H^\circ - T\Delta S^\circ \tag{8}$$

$$\Delta G^\circ = -RT\ln K_e \tag{9}$$

$$\ln K_e = \frac{\Delta S^\circ}{R} - \frac{\Delta H^\circ}{RT} \tag{10}$$

$$K_e = \frac{\alpha q_e}{C_e} \tag{11}$$

Where: R (J/mol·K) is the universal gas constant; K_e is the equilibrium constant, and α (g/L) the adsorbent concentration.

1.3 Modelling with Visual MINTEQ

Visual MINTEQ version 4.0 (4.07) is a Windows-based chemical equilibrium modelling software designed to simulate aqueous geochemical processes in both natural and engineered environments. Its core functionalities include calculating the speciation of dissolved metals, anions, and ligands in solution; modelling adsorption onto mineral surfaces using surface complexation models; simulating precipitation and dissolution reactions; estimating saturation indices to assess the likelihood of mineral formation or dissolution; and evaluating complexation and competitive interactions among multiple solutes (Zhang et al. 2025). In this study, Visual MINTEQ was primarily utilized to predict the aqueous speciation of Mn over a range of pH values, with the aim of identifying dominant species and elucidating potential geochemical reactions under varying conditions. Input parameters included solution pH, temperature, ionic strength, and the concentrations of major dissolved constituents. The model outputs provided detailed information on the total Mn concentration, the distribution and concentration of individual Mn species, their log activities, percentage contributions to the total Mn pool, and the saturation indices of relevant mineral phases.

2 Results and discussion

2.1 Characterization of Brown Coal (BC)

The characterization results of the BC are summarized in Table 1 and Figs. 1a–1d. As shown in

Table 1 Basic summary characteristics of the BC

Parameters	Value
pH_{pzc}	4.02
Moisture (%)	5.30
Ash content (%)	7.90
Volatile matter (%)	30.10
Fixed carbon (%)	56.70
Pore volume (cm^3/g)	0.017
Surface area (m^2/g)	6.70
Elemental composition (%)	
Carbon	65.68
Oxygen	24.61
Ca	2.00
Si	3.01
Al	2.37

Table 1, the proximate analysis revealed a moisture content of 5.3%, volatile matter of 30.10%, ash content of 7.90%, and fixed carbon of 56.70%. The moderate volatile matter content suggests the presence of thermally unstable organic compounds which, upon heating, contribute to pore formation, surface roughness, and the creation of additional adsorption sites. The ash content, representing the inorganic mineral fraction, can hinder pore accessibility when excessive but, in moderate amounts, may enhance ion exchange. The high fixed carbon content indicates a stable carbon matrix, favourable for metal ion retention via π–π interactions and surface complexation mechanisms. The specific surface area and total pore volume of the BC, measured by the BET method, were 6.7 m^2/g and 0.017 cm^3/g, respectively, which are consistent with those reported in the literature (e.g. Zhang et al. 2019; Jellali et al. 2021; Shi et al. 2024). The pH_{pzc} (Fig. 1a) was determined to be 4.02. This implies that the BC surface will be protonated and carries a net positive charge when the solution pH is below 4.02, which is unfavourable for cation adsorption. Conversely, above pH 4.02, the surface becomes deprotonated and negatively charged, facilitating the adsorption of positively charged metal ions. This pH_{pzc} value aligns with previously reported values for other BC materials (e.g. Jellali et al. 2021). X-Ray Diffraction (XRD) analysis (Fig. 1b) confirmed the presence of several mineral

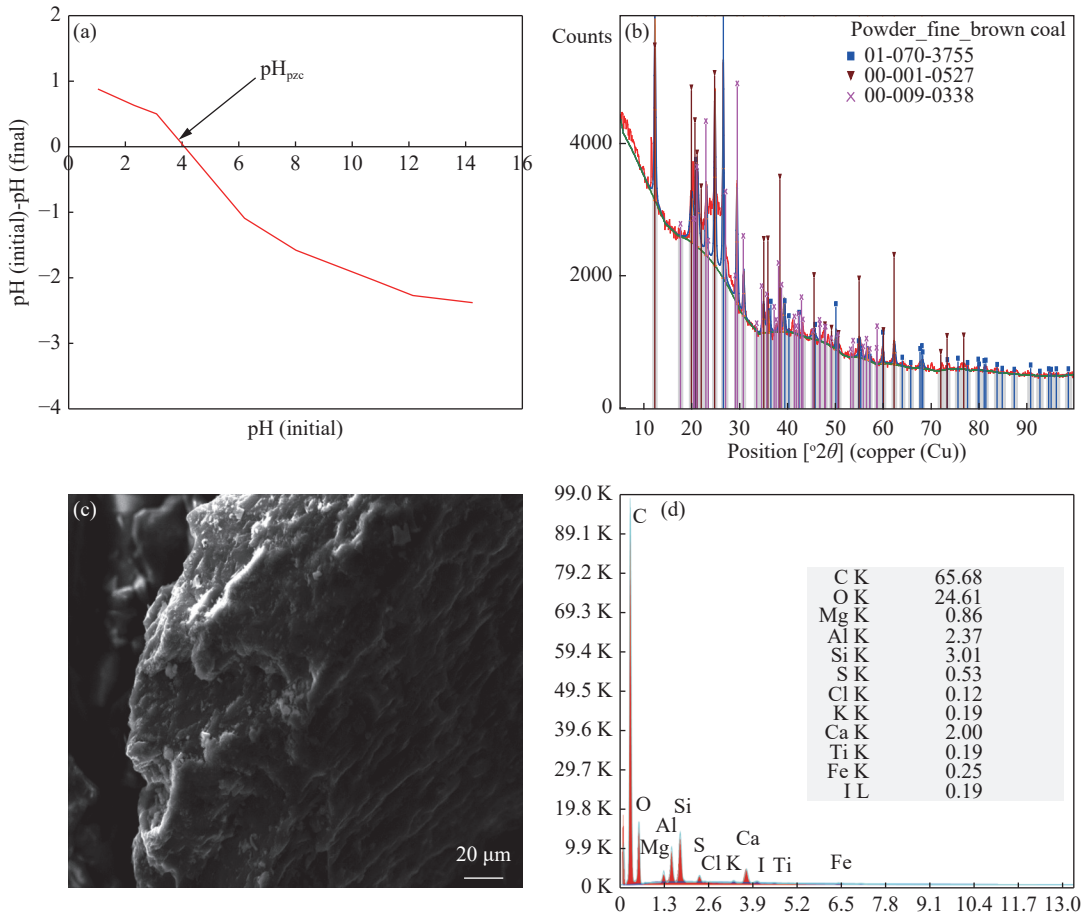

Fig. 1 Characterization results showing: (a) Point of zero charge, (b) X-ray diffraction spectrum, (c) SEM, and (d) EDX images of the unloaded BC

phases, including quartz (SiO_2), calcium carbonate ($CaCO_3$), kaolinite [$Al_2Si_2O_5(OH)_4$], and feldspar [$K(Na,K)_3\ Al_4Si_4O_{16}$]. These minerals possess reactive surface sites that may engage in chemical interactions with metal ions. Scanning Electron Microscopy (SEM) images (Fig. 1c) revealed a heterogeneous surface morphology with pores of irregular sizes and shapes. Energy Dispersive X-ray (EDX) analysis (Fig. 1d) showed the presence of various elements, including O, Si, Ca, Mg, K, Al, S, Cl, Ti, Fe and I in the BC, with carbon and oxygen being the predominant elements. These elements are likely associated with the silicate minerals present in the BC (Cui et al. 2016; Shi et al. 2024).

2.2 Effect of initial solution pH on Mn^{2+} adsorption

The initial solution pH plays a crucial role in the adsorption behaviour of metal ions by influencing both their speciation in solution and the surface charge of the adsorbent (Shi et al. 2024). To investigate this effect, batch adsorption experiments were conducted alongside geochemical modelling using Visual MINTEQ version 4.0. The modelling aimed to predict Mn speciation across varying pH levels and to elucidate the interactions between Mn^{2+} and the BC surface. As shown in Fig. 2, the efficiency of Mn^{2+} removal was strongly influenced by pH, as confirmed by both the experiments and modelling results. Specifically, removal efficiency increased sharply between pH 2 and pH 4, remained consistently high (ca. 90%–100%) from pH 4 to pH 10, and then declined slightly at pH values above 10. This trend reflects the interplay between solution chemistry and the surface charge dynamics of BC. At pH values below the pH_{pzc} of 4.02 (Fig. 1a), the high concentration of H^+

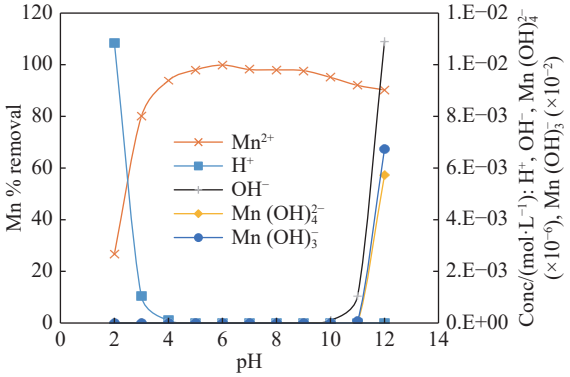

Fig. 2 Effect of initial solution pH on Mn^{2+} removal by BC

ions compete with Mn^{2+} for available surface binding sites, resulting in reduced adsorption. Additionally, the BC surface is protonated and thus positively charged under acidic conditions, resulting in electrostatic repulsion of the divalent Mn^{2+} ions (Eq. 12). As pH increases above the pH_{pzc}, deprotonation of functional groups on the BC surface occurs (Eqs. 13), rendering the surface negatively charged and promoting Mn^{2+} uptake via electrostatic attraction, ion exchange, and surface complexation (Eq. 14). The optimal pH range for Mn^{2+} removal was identified as 4–10, within which Mn^{2+} remains predominantly in its free ions form, facilitating its effective interaction with the adsorbent. At pH values above 10.5, Mn begins to hydrolyse, forming species such as $Mn(OH)_4^{2-}$ and $Mn(OH)_3$. These hydrolysed species are less favourable for adsorption or may precipitate from solution, accounting for the observed decline in removal efficiency at higher pH levels.

$$BC-COOH+H^+ \leftrightarrow \underbrace{BC-COOH_2^+}_{\substack{\text{Protonation of BC surface}\\ \text{resulting in electrostactic}\\ \text{repulsion of } Mn^{2+}}} \quad (12)$$

$$BC-COOH+OH^- \leftrightarrow \underbrace{BC-COO^-}_{\substack{\text{Deprotonation of BC surface}\\ \text{favouring adsorption}\\ \text{of } Mn^{2+}}} +H_2O \quad (13)$$

$$nBC\_COO^- + Metal_{(aq)}^{n+} \leftrightarrow (BC-COO)_n\ Metal \quad (14)$$

2.3 Effect of BC dosage and initial Mn^{2+} concentration

The impact of BC dosage on Mn^{2+} adsorption was studied under initial conditions of 10 mg/L Mn^{2+}, at 298 K and pH 6. As shown in Fig. 3a, the removal efficiency increased from 42% to 98.09% as the BC dosage increased from 0.2 g to 1 g (Fig. 3a). This trend aligns with previous findings (Jellali et al. 2021) and is primarily attributed to the greater availability of adsorption sites at higher BC dosage (Siri-Anusornsak et al. 2024). However, further increases in BC dosage beyond 1 g did not lead to a substantial improvement in Mn^{2+} removal. The specific adsorption capacity (mg/g) decreased as the BC dosage increased, a phenomenon that may be attributed to potential pore occlusion or particle aggregation at higher sorbent loadings, which can reduce the effective surface area available for adsorption (Xu et al.

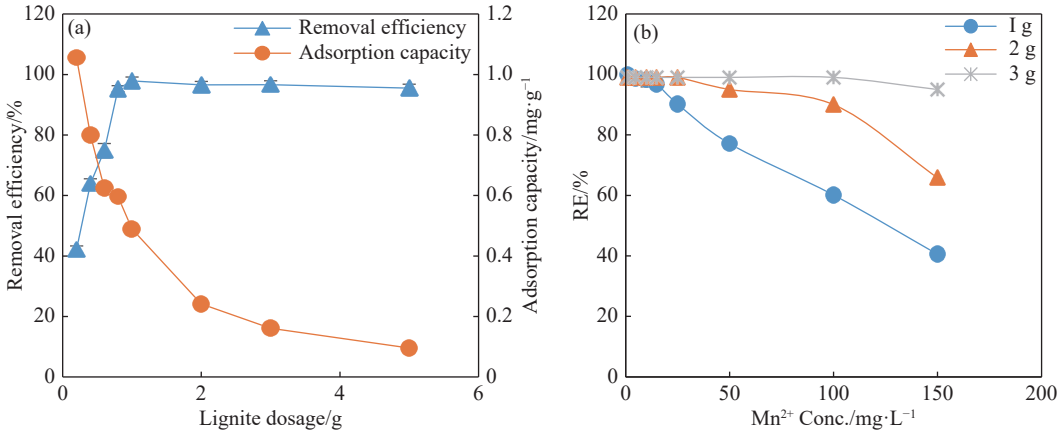

Fig. 3 The impact of (a) BC dosage and (b) initial Mn^{2+} concentration on Mn^{2+} adsorption

2017). As noted by Siri-Anusornsak et al. (2024), increasing the adsorbent mass at a constant volume of solution may also promote agglomeration, thereby reduce the overall surface area and elongate diffusional pathways, which can adversely affect adsorption efficiency.

The combined effects of varying initial Mn^{2+} concentrations and different BC dosages were further investigated. As illustrated in Fig. 3b, removal efficiency decreased with increasing Mn^{2+} concentration rose (from 1 mg/L to 150 mg/L) across all three BC dosages. This decrease likely resulted from the higher ratio of available adsorption sites to adsorbate concentration at lower concentrations, facilitating rapid and thorough removal. Conversely, at higher concentrations, the fixed number of adsorption sites becomes saturated, leading to reduced removal efficiency (Kurniasih et al. 2025). Although the influence of the BC dosage on Mn^{2+} removal was more subtle at lower concentrations, its influence became increasingly evident at higher at Mn^{2+} concentration increases, emphasizing the need of optimize adsorbent dosage for effective treatment of heavily contaminated water.

2.4 Effect of coexisting ions

The presence of Coexisting Ions (CIs) in surface and subsurface water environments can significantly influence the adsorption of target contaminants (Efome et al. 2019). Depending on their interactions with the target contaminant and the adsorbent, CIs may exert one of three distinct effects: (1) A synergistic effect, where the presence of CI enhances adsorption and thus increases removal efficiency; (2) An antagonism (inhibitory) effect, where CI competes with the target contaminant for active adsorption sites, thereby reducing adsorption efficiency; or (3) No interaction, where the CI has negligible influence on the adsorption process, indicating minimal competitive behaviour (Macena et al. 2025). Understanding these effects is essential for optimizing adsorption-based remediation strategies and predicting contaminant behaviour in complex aquatic systems. In this study, the influence of six common cations, Na^+, K^+, Ca^{2+}, Cu^{2+}, Zn^{2+}, and Fe^{3+}, on Mn^{2+} adsorption was investigated under binary systems at concentrations of 5, 10, and 15 mg/L. As illustrated in Figs. 4a–4e, the presence of Ca^{2+}, Na^+, and K^+ generally led to their release into the solution, suggesting that ion-exchange processes occurred between Mn^{2+} and these competing cations. Compared to the single-ion system (Mn^{2+} only), Mn^{2+} removal efficiency was consistently lower in the presence of the CI (binary systems), and this reduction became more pronounced with increasing CI concentrations. This decline is attributed to direct competition for adsorption sites and an increase in ionic strength of the solution, which likely compressed the electrical double layer surrounding the BC particles and weakened electrostatic interactions essential for adsorption. Among the tested ions, monovalent cations (Na^+ and K^+) exhibited a relatively weaker influence on Mn^{2+} adsorption than divalent (Ca^{2+}, Cu^{2+}, Zn^{2+}) and trivalent (Fe^{3+}) cations. Notably, Fe^{3+} and Cu^{2+} had the strongest antagonistic effects, significantly suppressing Mn^{2+} uptake. This can be explained by their higher charge densities, greater electronegativities, and smaller hydrated ionic radii, which enhance their affinity for adsorption sites over Mn^{2+} (Yao et al. 2020; Jellali et al. 2021; Kim et al. 2021).

2.5 Mn^{2+} adsorption thermodynamics

The thermodynamic parameters-ΔG°, ΔH°, and ΔS°- analysed in this study are presented in Table

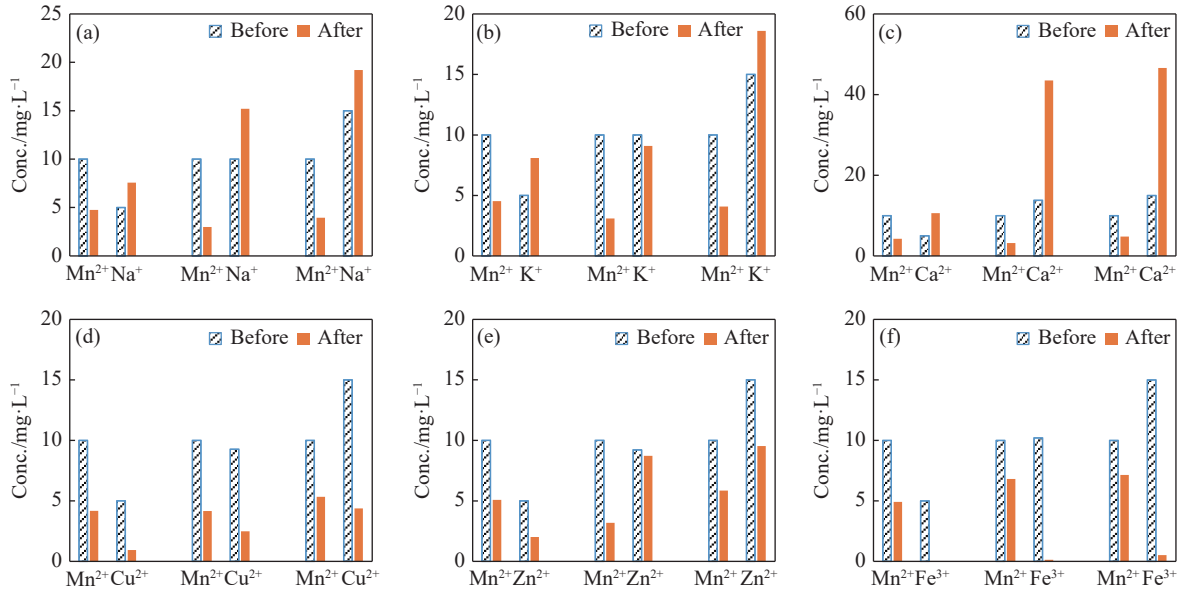

Fig. 4 Effect of coexisting ions (Na^+, K^+, Ca^{2+}, Cu^{2+}, Zn^{2+}, Fe^{3+} at concentrations of 5 mg/L, 10 mg/L, and 15 mg/L) on Mn^{2+} adsorption by BC

2. The negative ΔG° values confirm that Mn^{2+} adsorption onto the BC is spontaneous and thermodynamically favourable (Sahmoune, 2019). Moreover, the increasingly negative ΔG° values with rising temperature suggest that the adsorption process becomes more efficient at elevated temperatures. This trend is likely due to increased kinetic energy of the Mn^{2+} ions, leading to more frequent and effective collisions with the active sites on the BC surface (Quansah et al. 2024). The positive value of ΔH° (15.53 kJ/mol) indicates that the adsorption process is endothermic, requiring energy input to proceed (Sahmoune, 2019), while the positive ΔS° value indicates that randomness of the system increases during the adsorption process (Sahmoune, 2019; Quansah et al. 2024).

Table 2 Thermodynamic parameters for Mn^{2+} adsorption on BC

Temperature K	ΔG° kJ/mol	ΔH° kJ/mol	ΔS° kJ/mol-K
298	−4.89	15.53	0.069
323	−6.73		
348	−8.42		
363	−9.12		
373	−10.08		
393	−11.55		

2.6 Sorption isotherms

In the present study, the Freundlich (Fig. 5a) and Langmuir (Fig. 5b) equilibrium isotherm models were utilized to further characterize Mn^{2+} adsorption onto the BC. Both models provided excellent fits to the experimental data, with correlation coefficients of R^2 = 0.994 for the Langmuir and R^2 = 0.993 for the Freundlich isotherm, indicating that Mn^{2+} adsorption onto BC may involve a combination of homogeneous and heterogeneous surface interactions. The Freundlich isotherm yielded 1/n value of 0.85, suggesting favourable adsorption conditions (Fseha et al. 2022). The separation factor (R_L) determined from the Langmuir isotherm (using Eq. 14) also confirmed the favourability of the adsorption process

$$R_L=\frac{1}{[1+(K_L\times C_0)]} \tag{15}$$

Where: K_L (L/mg) is the Langmuir adsorption constant (0.018 L/mg), C_0 is the initial Mn^{2+} concentration. The calculated R_L values ranged from 0.53 to 0.98, which falls between 0 and 1 (Quansah et al. 2024). An $R_L < 1$ indicates favourable adsorption; $R_L = 0$ indicates irreversible adsorption; $R_L = 1$ is linear adsorption; and $R_L > 1$ suggests unfavourable adsorption. The Langmuir isotherm analysis yielded a maximum adsorption capacity (Q_{max}) of 1.19 mg/g, demonstrating that BC performs as well as, or better than, some natural adsorbents (Table 3). These findings support the viability of BC as an effective sorbent for Mn^{2+} removal from contaminated groundwater.

2.7 Sorption kinetics

Fig. 6a illustrates the time-dependent adsorption

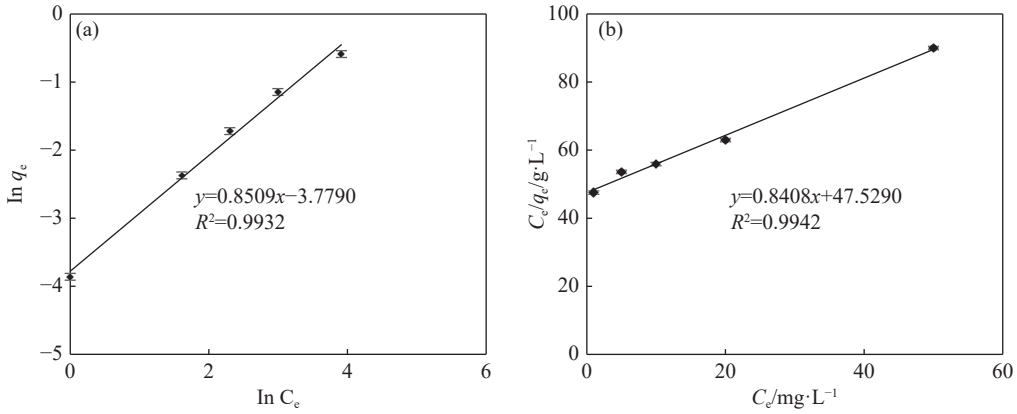

Fig. 5 Mn^{2+} experimental data fitted with (a) Freundlich and (b) Langmuir isotherms

Table 3 Comparison of Mn^{2+} adsorption capacity (Q_{max}) obtained in this study with those reported for other natural and low-cost adsorbents in previous studies

Adsorbent	Q_{max}/mg/g	Particle size	pH	Temperature/°C	Reference
Zeolite Y	0.015	0.75 μm	6.50	25	Kwakye-Awuah et al. 2019
Phoenix dactylifera L. seed	0.361	NA	7.0	NA	Osundiya et al. 2024
Date palm biochar	0.44	0.15 mm	6	NA	Fseha et al. 2022
Tea waste	0.158	2 mm	NA	NA	Badrealam et al. 2019
BC	1.190	75 μm	6.00	25	This study

Q_{max}: Maximum adsorption capacity; NA = not available

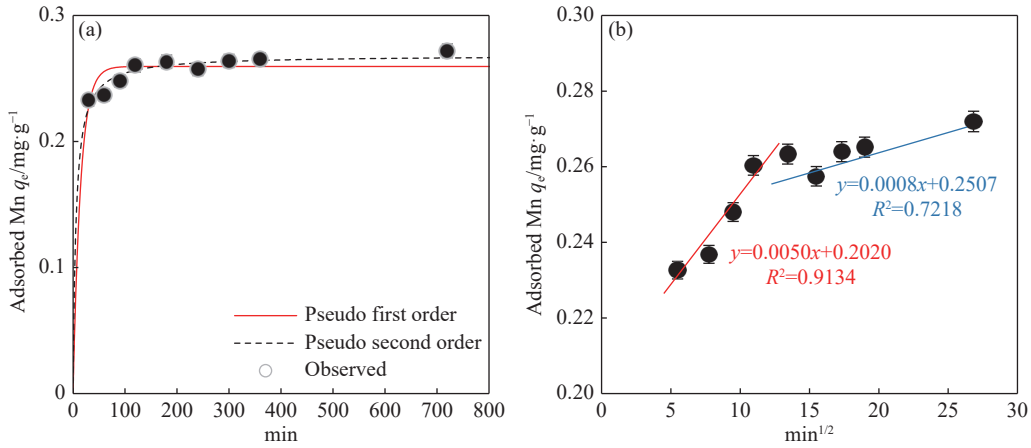

Fig. 6 Evaluation of Mn^{2+} adsorption kinetic data with (a) pseudo-first-order and pseudo-second-order models and (b) the intra-particle diffusion model

behaviour of Mn^{2+} onto BC. A rapid increase in Mn^{2+} uptake was observed within the first 30 minutes, followed by a gradual approach to equilibrium, which was reached at approximately 120 minutes. The initial rapid phase is attributed to the immediate occupation of easily accessible surface sites, `while the slower phase reflects the adsorption on less accessible sites and the diffusion of Mn^{2+} ions into the BC micropores (Shi et al. 2024). To model the adsorption kinetics, both Pseudo-First-Order (PFO) kinetic and Pseudo-Second-Order (PSO) kinetic models were applied. As depicted in Table 4 and Fig. 6a, both models fitted to the experimental data well, though the PSO kinetic model more accurately predicted the equilibrium adsorption capacity, suggesting a chemisorption process. Adsorption kinetics often involve multiple steps, including Intra-Particle Diffusion (IPD) and mass transfer across boundary layers. To further understand the adsorption mechanisms, the IPD model was applied. The IPD suggests that if a plot of q_t against $t^{1/2}$ is linear and passes through

Table 4 Parameters of the PFK, PSK and IPD models

PFK			PSK			IPD			
q_e (mg/g)	k_1 (1/h)	R^2	q_e (mg/g)	k_2 (mg/g h)	R^2	k_{p1} (mg/g $min^{1/2}$)	R^2	k_{p2} (mg/g $min^{1/2}$)	R^2
0.259	0.070	0.988	0.268	0.673	0.996	0.005	0.913	0.0008	0.722

the origin, IPD is considered the sole rate- controlling mechanism. As shown in Fig. 6b, the plot displayed two linear distinct phases, neither of which passes through the origin, indicating a complex adsorption process involving more than just IPD (Quansah et al. 2024).

2.8 Reusability and environmental benignity of Brown Coal (BC)

The reusability of an adsorbent is a critical parameter for evaluating its practical applicability. An ideal reusable material should maintain its structural integrity and adsorption efficiency over multiple regeneration cycles, while also remaining easy to handle without significant material loss or degradation (Kolya and Kang, 2025). As shown in Fig. 7a, the adsorption efficiency of Brown Coal (BC) decreased slightly from 91.99% to 84.61% after four consecutive adsorption–desorption cycles. The sustained performance highlights BC's potential as a reusable adsorbent and can be attributed to its high fixed carbon content, which enhances mechanical strength and chemical stability, reducing the risk of structural breakdown or oxidative degradation during repeated use. In addition, the moderate ash content may provide stable mineral phases that support ion exchange capacity throughout reuse. However, the observed decline in adsorption efficiency over successive cycles may be attributed to factors such as incomplete Mn^{2+} desorption, loss of fine BC particles during washing, pore blockage, or alterations in surface functional groups over time (Quansah et al. 2024; Sithole, 2024). In addition to reusability, evaluating the environmental compatibility of natural adsorbents is essential to ensure that their application does not result in unintended secondary pollution, a phenomenon commonly referred to as pollution swapping. Pollution swapping occurs when efforts to remove a target contaminant led to the release or increase of of other pollutants (Zhan et al. 2024). To assess this risk, the concentrations of Heavy Metals (HMs)—including Cu, Zn, Cd, Pb, Cr, and Fe—were analysed in Mn-contaminated groundwater before and after the addition of BC. As shown in Fig. 7b, the initial concentrations of these HMs in untreated water were low. After BC addition, Zn concentrations exhibited a slight increase, while Cd and Fe concentrations decreased. The levels of Pb, Cu, and Cr remained unchanged. Importantly, all measured HMs concentrations remained below the WHO permissible limits: Cu (2 mg/L), Zn (2 mg/L), Cd (0.003 mg/L), Pb (0.01 mg/L), Cr (0.05 mg/L), and Fe (0.3 mg/L). These findings suggest that the use of BC does not pose a significant environmental risk and can be considered a safe and sustainable adsorbent for the remediation of Mn-contaminated groundwater.

2.9 Mn^{2+} sorption mechanisms

The removal of heavy metals by BC has been extensively studied and is known to proceed via multiple mechanisms, with ion exchange and surface complexation being the most dominant pathways (Jellali et al. 2021; Hu et al. 2024). Ion

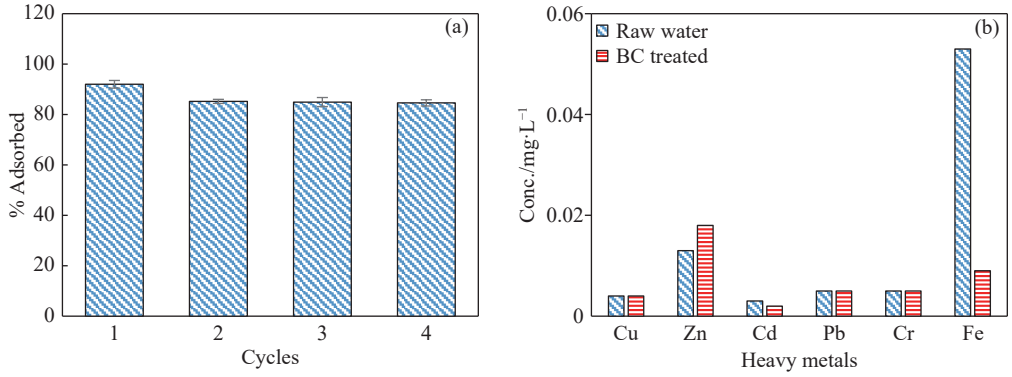

Fig. 7 Results of experiments to study (a) the reusability of the BC, and (b) the environmental benignity of the BC (Adsorbent mass: 1 g; pH = 6)

exchange typically involves the replacement of exchangeable ions on the adsorbent by incoming metal ions in equimolar proportions to maintain electrostatic neutrality. This process is often referred to as outer-sphere surface complexation, where the exchanged ions reside in the secondary coordination shell of the metal-ligand complex (Nadagouda et al. 2024). In this study, the stoichiometric relationship between the amount of adsorbed Mn^{2+} ions and the concomitant release of major cations (Ca^{2+}, Mg^{2+}, Na^{+}, and K^{+}) into solution was evaluated to determine the contribution of ion exchange to Mn^{2+} removal by BC. As illustrated in Fig. 8a, Mn^{2+} adsorption increases with rising pH, particularly between pH 4 and pH 6, which corresponds with a marked release of Ca^{2+} and Mg^{2+} into the solution. These cations likely originated from the mineral constituents of BC, such as quartz, calcium carbonate, kaolinite, and feldspar, as confirmed by XRD analysis and the measured ash content (7.90%). Notably, the concentrations of Ca^{2+} and Mg^{2+} peaked at pH 2, reaching approximately 45 mg/L and 20 mg/L, respectively, suggesting they are primary ions displaced during Mn^{2+} adsorption. In contrast, the release of Na^{+} and K^{+} was minimal, indicating their limited iinvolvement in the ion exchange process, possibly due to their stronger retention or lower

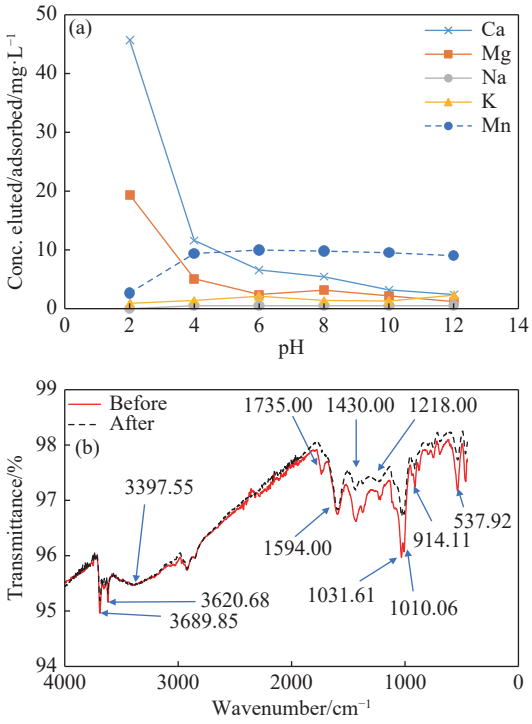

Fig. 8 (a) Net concentrations of Ca^{2+}, Na^{+}, Mg^{2+}, K^{+} and Mn^{2+} eluted/adsorbed into solution at different solution pH values, and (b) FTIR spectra of the BC before and after loading with Mn^{2+}

availability on the BC surface (Quansah et al. 2024). However, a comparison of the total molar concentrations of the displaced cations with the moles of Mn^{2+} adsorbed at equilibrium reveals that the Mn^{2+} uptake exceeds the total released cations, particularly at higher pH values. This non-stoichiometric relationship suggests that ion exchange alone cannot account for the observed removal, and other mechanisms, most likely surface complexation, play a substantial role. Surface complexation, particularly inner-sphere complex complexation, involves the direct coordination of metal ions with surface functional groups on the adsorbent surface, without requiring the displacement of pre-bound cations. This aligns with the observed non-equimolar ion release, implying the simultaneous operation of ion exchange and surface complexation during Mn^{2+} removal.

To further investigate the complexation mechanism, Fourier Transform Infrared (FTIR) spectroscopy was performed at pH 6. The spectra revealed significant shifts in functional group vibrations, indicative of chemical interactions between the BC surface and Mn^{2+}. In the high wavenumber region (3,689.85 cm^{-1}, 3,620.68 cm^{-1}, and 3,397.55 cm^{-1}), broad bands associated with O–H stretching were observed, suggesting the involvement of hydroxyl groups or adsorbed water in Mn^{2+} binding. These bands exhibited slight shifts and intensity changes after Mn^{2+} exposure, pointing to their role in surface complexation via hydrogen bonding or direct coordination. Further spectral evidence was observed at 1,735 cm^{-1} and 1,594 cm^{-1}, corresponding to C=O stretching (carbonyl groups) and asymmetric COO^{-} vibrations, respectively. These peaks showed notable shifts, indicating that carboxyl groups participate in Mn^{2+} complexation. Additional changes at 1,430 cm^{-1} and 1,218 cm^{-1}, related to C–H bending and symmetric COO^{-} stretching, respectively, further support the role of carboxyl groups in Mn^{2+} binding. In the fingerprint region (1,031.61–914.11 cm^{-1}), alterations in peaks corresponding to Si–O–Si and Si–O–Al stretching vibrations suggest interactions between Mn^{2+} and the silicate or aluminosilicate matrix of BC. Moreover, the emergence or enhancement of a peak near 537.92 cm^{-1}, associated with Metal–Oxygen (M–O) vibrations, confirms the formation of direct Mn–O bonds, characteristic of inner-sphere complexation rather than weak electrostatic interactions. In summary, the combination of non-stoichiometric ion exchange data and FTIR spectral shifts strongly supports the conclusion that both ion exchange and surface complexation (particularly

inner-sphere complexation) are key mechanisms in Mn^{2+} removal by BC.

2.10 Removal of Mn^{2+} from real Mn^{2+}–contaminated groundwater

Evaluating the effectiveness of adsorbents for groundwater treatment requires testing under both simulated and real groundwater conditions. Simulated groundwater facilitates the assessment of individual parameters under controlled conditions, while real groundwater provides a more comprehensive understanding of how various constituents interact under natural conditions. This dual approach ensures that the adsorption process is both scientifically valid and practically applicable. Table 5 highlights the physico-chemical properties of real groundwater before and after treatment with BC. The pH, turbidity, colour, Fe, and Mn were the main parameters of concern in the groundwater. Treatment with BC significantly reduced turbidity (from 59.2 NTU to 2.09 NTU), colour (from 75 Hz to 5 Hz), total iron (from 18.0 mg/L to 0.401 mg/L), and Mn^{2+} (from 10.2 mg/L to 1.14 mg/L). This corresponds to a Mn removal efficiency of 88.82%, which, although slightly lower than that observed in the simulated system, remains highly effective. This can be attributed to the competition from other ions, as observed in the binary system experiments. Conversely, slight increases were observed in certain parameters following BC treatment. pH increased from 6.21 to 6.57, electrical conductivity rose from 531 µS/cm to 623 µS/cm, and total dissolved solids increased from 293 mg/L to 343 mg/L. These changes are consistent with the the ion exchange mechanisms, wherein ions like Na^{+}, Cl^{-}, and Ca^{2+} are released from the BC into solution. Similarly, total hardness increased marginally from 150 mg/L to 157 mg/L, and calcium hardness rose from 60.1 mg/L to 72.3 mg/L, indicating a probable exchange of magnesium ions for calcium ions during the adsorption process. Despite these increases, the concentrations of these parameters remained well within the WHO recommended limits. These findings confirm that BC is not only effective in removing Mn^{2+} from contaminated groundwater but also has a manageable impact on secondary water quality parameters, affirming its potential for practical application in sustainable water treatment systems

3 Conclusion

This study demonstrated the effectiveness of Brown Coal (BC) in removing Mn^{2+} from simulated and real contaminated groundwater, underscoring its potential for practical application in groundwater remediation. The adsorption process was influenced by several operational parameters,

Table 5 Physico-chemical properties of real groundwater before and after BC treatment

Parameter	Unit	Before BC	After BC	WHO (2017)
Turbidity	NTU	59.2	2.09	5
Colour (apparent)	Hz	75.0	5.00	5
pH	pH Units	6.21	6.57	6.5–8.5
Conductivity	µS/cm	531	623	-
TSS	mg/l	49.0	1.00	-
TDS	mg/l	293	343	1,000
Sodium	mg/l	16.0	56.0	200
Potassium	mg/l	6.00	3.30	30
Calcium	mg/l	24.0	28.9	200
Magnesium	mg/l	21.7	20.7	150
Total Iron	mg/l	18.0	0.401	0.3
Ammonium (NH_4-N)	mg/l	0.001	<0.001	0.00–1.5
Chloride	mg/l	76.9	185	250
Sulphate (SO_4)	mg/l	18.7	16.10	250
Manganese	mg/l	10.20	1.14	0.4
Nitrite (NO_2-N)	mg/l	0.036	<0.001	1
Nitrate (NO_3-N)	mg/l	0.111	0.247	10
Total Hardness (as $CaCO_3$)	mg/l	150	157	500
Bicarbonate (as $CaCO_3$)	mg/l	77.6	14.4	-

including solution pH, adsorbent dosage, contact time, temperature, and initial Mn^{2+} concentration. Equilibrium was rapidly achieved within 30 minutes, with optimal removal efficiency observed at pH 6. The maximum Mn^{2+} adsorption capacity of BC was determined to be 1.19 mg/g, which is comparable to or exceeds the performance of many other natural adsorbents reported in the literature. Thermodynamic analysis confirmed that the adsorption process was spontaneous and endothermic, with increased temperatures enhancing Mn^{2+} removal efficiency. BC also exhibited excellent reusability, maintaining high adsorption performance over four successive adsorption–desorption cycles. Furthermore, leached ions from the BC remained within acceptable limits for potable water, affirming its environmental safety. However, the presence of coexisting ions—particularly divalent and trivalent cations such as Ca^{2+}, Cu^{2+}, Zn^{2+}, and Fe^{3+}—negatively impacted Mn^{2+} removal due to competition for active adsorption sites. The extent of this interference is dependent on ion charge density and concentration. Mechanistic analysis revealed that Mn^{2+} removal was primarily governed by ion exchange involving Ca^{2+}, Mg^{2+}, K^{+}, and Na^{+}, as well as surface complexation, notably through inner-sphere complex formation with surface functional groups on the BC. Overall, these findings highlight BC as a cost-effective, reusable, and environmentally benign adsorbent with strong potential for sustainable groundwater treatment applications targeting Mn^{2+} and similar contaminants.

References

Badrealam S, Darrell VC, Dollah Z, et al. 2019. Adsorption of manganese and zinc in synthetic wastewater by tea waste (TW) as a low-cost adsorbent. Journal of Physics: Conference Series, 1349(1): 012061. DOI：10.1088/1742-6596/1349/1/012061.

Biney E, Mintah BA, Ankomah E, et al. 2024. Sustainability assessment of groundwater in south-eastern parts of the western region of Ghana for water supply. Cleaner Water, 1: 100007. DOI：10.1016/j.clwat.2024.100007.

Caldwell RW, Rodriguez PC, Toque HA, et al. 2018. Arginase: A multifaceted enzyme important in health and disease. Physiological reviews, 98(2): 641−665. DOI：10.1152/physrev.00037.2016.

Çalışır A, Yavuz SÇ, Yavuz E, et al. 2024. Removal of manganese (Mn^{2+}) from water samples using a biocomposite sorbent. Environmental Research, 257: 119353. DOI：10.1016/j.envres.2024.119353.

Chen JJ, Tao L, Liu BX, et al. 2024. Distribution characteristics and origin analysis of iron and manganese in groundwater in Beijing Plain Area. Hydrogeology & Engineering Geology, 51(6): 198−207. DOI：10.16030/j.cnki.issn.1000-3665.202311051.

Chen X, Hossain M, Duan C, et al. 2022. Isotherm models for adsorption of heavy metals from water-A review. Chemosphere, 307: 135545. DOI：10.1016/j.chemosphere.2022.135545.

Cui X, Fang S, Yao Y, et al. 2016. Potential mechanisms of cadmium removal from aqueous solution by Canna indica derived biochar. Science of the Total Environment, 562: 517−525. DOI：10.1016/j.scitotenv.2016.03.248.

Debrah SK, Issahaku T, Obiri-Nyarko F, et al. 2024. Hydrogeochemical characterization and spatial analysis of groundwater quality in the Bono East Region, Ghana. International Journal of Energy and Water Resources, 1-18. DOI: 10.1007/s42108-024-00322-y

Efome JE, Rana D, Matsuura T, et al. 2019. Effects of operating parameters and coexisting ions on the efficiency of heavy metal ions removal by nano-fibrous metal-organic framework membrane filtration process. Science of the Total Environment, 674: 355−362. DOI：10.1016/j.scitotenv.2019.04.187.

Fseha YH, Sizirici B, Yildiz I. 2022. Manganese and nitrate removal from groundwater using date palm biochar: Application for drinking water. Environmental Advances, 8: 100237. DOI：10.1016/j.envadv.2022.100237.

Galangashi MA, Kojidi SFM, Pendashteh A, et al. 2021. Removing iron, manganese and ammonium ions from water using greensand in fluidized bed process. Journal of Water Process Engineering, 39: 101714. DOI：10.1016/j.jwpe.2020.101714.

Hu J, Han B, Butterly CR, et al. 2024. Catalytic oxidation of lignite by Pt/TiO_2 can enhance cadmium adsorption capacity. Journal of Hazardous Materials, 465: 133207. DOI：10.1016/j.jhazmat.2023.133207.

Jakariya M, Rahman MM, Mahzabin L, et al.

2024. Developing a safe water atlas for sustainable drinking water supply in Sonargaon Upazila, Bangladesh. Groundwater for Sustainable Development, 25: 101126. DOI：10.1016/j.gsd.2024.101126.

Jellali S, Azzaz AA, Jeguirim M, et al. 2021. Use of lignite as a low-cost material for cadmium and copper removal from aqueous solutions: Assessment of adsorption characteristics and exploration of involved mechanisms. Water, 13(2): 164. DOI：10.3390/w13020164.

Jiang L, Cheng Y, Huang T, et al. 2023. Removal of manganese from water by modified groundwater plant sludge: Mechanism and application as filter media. Journal of Water Process Engineering, 51: 103418. DOI：10.1016/j.jwpe.2022.103418.

Kim S, Gholamirad F, Yu M, et al. 2021. Enhanced adsorption performance for selected pharmaceutical compounds by sonicated Ti3C2TX MXene. Chemical Engineering Journal, 406: 126789. DOI：10.1016/j.cej.2020.126789.

Kobielska PA, Howarth AJ, Farha OK, et al. 2018. Metal–organic frameworks for heavy metal removal from water. Coordination Chemistry Reviews, 358: 92−107. DOI：10.1016/j.ccr.2017.12.010.

Kolya H, Kang CW. 2025. Recent advances in polymer nanocomposites for the adsorptive removal of toxic azo dyes from water. Discover Water, 5(1): 28. DOI：10.1007/s43832-025-00217-x.

Kurniasih M, Aprilita NH, Roto R, et al. 2025. Modification of coal fly ash for high-capacity adsorption of methylene blue. Case Studies in Chemical and Environmental Engineering, 11: 101101. DOI：10.1016/j.cscee.2025.101101.

Kwakye-Awuah B, Sefa-Ntiri B, Von-Kiti E, et al. 2019. Adsorptive removal of iron and manganese from groundwater samples in Ghana by zeolite Y synthesized from bauxite and kaolin. Water, 11(9): 1912. DOI：10.3390/w11091912.

Macena M, Pereira H, Cruz-Lopes L, et al. 2025. Competitive adsorption of metal ions by lignocellulosic materials: A review of applications, mechanisms and influencing factors. Separations, 12(3): 70. DOI：10.3390/separations12030070.

McKinley K, McLellan I, Gagné F, et al. 2019. The toxicity of potentially toxic elements (Cu, Fe, Mn, Zn and Ni) to the cnidarian *Hydra attenuata* at environmentally relevant concentrations. Science of the Total Environment, 665: 848−854. DOI：10.1016/j.scitotenv.2019.02.193.

Nadagouda MN, Varshney G, Varshney V, et al. 2024. Recent advances in technologies for phosphate removal and recovery: A review. ACS Environmental Au, 4(6): 271−291. DOI：10.1021/acsenvironau.3c00069.

Neculita CM, Rosa E. 2019. A review of the implications and challenges of manganese removal from mine drainage. Chemosphere, 214: 491−510. DOI：10.1016/j.chemosphere.2018.09.106.

Obiri-Nyarko F, Kwiatkowska-Malina J, Kumahor SK, et al. 2022. Evaluating low-cost permeable adsorptive barriers for the removal of benzene from groundwater: Laboratory experiments and numerical modelling. Journal of Contaminant Hydrology, 250: 104054. DOI：10.1016/j.jconhyd.2022.104054.

Osundiya M, Sobola A, Oyewole T, et al. 2024. Kinetics, isotherms and thermodynamics studies of Pb^{2+} and Mn^{2+} adsorption from model wastewater solution using raw Phoenix dactylifera L. seed. Journal of Research and Review in Science, 11: 30−46. DOI：10.36108/jrrslasu/4202.11.0192.

Panagopoulos A, Michailidis P. 2025. Membrane technologies for sustainable wastewater treatment: Advances, challenges, and applications in zero liquid discharge (zld) and minimal liquid discharge (mld) systems. Membranes, 15(2): 64. DOI：10.3390/membranes15020064.

Quansah JO, Obiri-Nyarko F, Karikari AY. 2024. Adsorptive removal of dissolved iron from groundwater by brown coal–A low-cost adsorbent. Journal of Contaminant Hydrology, 260: 104283. DOI：10.1016/j.jconhyd.2023.104283.

Rudi NN, Muhamad MS, Te Chuan L, et al. 2020. Evolution of adsorption process for manganese removal in water via agricultural waste adsorbents. Heliyon, 6(9): e05049. DOI: 10.1016/j.heliyon.2020.e05049

Sahmoune MN. 2019. Evaluation of thermodynamic parameters for adsorption of heavy metals by green adsorbents. Environmental Chemistry Letters, 17(2): 697−704. DOI：10.1007/s10311-018-00819-z.

Shi Z, Wu C, Wang F, et al. 2024. Adsorption performance and mechanism of Fe (II) adsorption in abandoned mine water of nonstick coal. Processes, 12(1): 188. DOI：10.3390/pr12010188.

Siri-Anusornsak W, Kolawole O, Soiklom S, et al. 2024. Innovative use of spirogyra sp biomass for the sustainable adsorption of aflatoxin B1 and ochratoxin A in aqueous solutions. Molecules, 29(21): 5038. DOI：10.3390/molecules29215038.

Sithole T. 2024. A review on regeneration of adsorbent and recovery of metals: Adsorbent disposal and regeneration mechanism. South African Journal of Chemical Engineering, 50(1): 39-50. DOI: 10.1016/j.sajce.2024.07.006

Sönmez D, Hocaoğlu Ç. 2023. Manganese intoxication presenting with depressive symptoms: A case report. Archives of Neuropsychiatry, 60(3): 288. DOI：10.29399/npa.28305.

Sun M, Gu S, Liu X, et al. 2023. Adsorption mechanism of ammonia nitrogen and phenol on lignite surface: Molecular dynamics simulations and quantum chemical calculations. Fuel, 337: 127157. DOI：10.1016/j.fuel.2022.127157.

Tabi RN, Gibrilla A, Boakye P, et al. 2024. Appraisal of groundwater quality and hydrochemistry in three regions of Ghana: Implications for drinking purposes. Groundwater for Sustainable Development, 26: 101193. DOI：10.1016/j.gsd.2024.101193.

Tu Y, Feng P, Ren Y, et al. 2019. Adsorption of ammonia nitrogen on lignite and its influence on coal water slurry preparation. Fuel, 238: 34−43. DOI：10.1016/j.fuel.2018.10.085.

Virolainen S, Wesselborg T, Kaukinen A, et al. 2021. Removal of iron, aluminium, manganese and copper from leach solutions of lithium-ion battery waste using ion exchange. Hydrometallurgy, 202: 105602. DOI：10.1016/j.hydromet.2021.105602.

Wang J, Guo X. 2020. Adsorption kinetic models: Physical meanings, applications, and solving methods. Journal of Hazardous materials, 390: 122156. DOI：10.1016/j.jhazmat.2020.122156.

WHO. 2017. World Health Organization. Guidelines for drinking-water quality: First addendum to the fourth edition.

Xu P, Zeng GM, Huang DL, et al. 2017. Fabrication of reduced glutathione functionalized iron oxide nanoparticles for magnetic removal of Pb (II) from wastewater. Journal of the Taiwan Institute of Chemical Engineers, 71: 165−173. DOI：10.1016/j.jtice.2016.11.031.

Yao N, Li C, Yu J, et al. 2020. Insight into adsorption of combined antibiotic-heavy metal contaminants on graphene oxide in water. Separation and Purification Technology, 236: 116278. DOI：10.1016/j.seppur.2019.116278.

Zhan X, Zhang Q, Li M, et al. 2024. The shape of reactive nitrogen losses from intensive farmland in China. Science of the Total Environment, 915: 170014. DOI：10.1016/j.scitotenv.2024.170014.

Zhang H, Li Q, Zhao M, et al. 2025. Leaching law of heavy metals in coal gangue: A combination of experimental optimization and simulation. Journal of Hazardous Materials, 484: 136790. DOI：10.1016/j.jhazmat.2024.136790.

Zhang X, Zhou JW, Wang XJ, et al. 2025. Removal process of iron and manganese ions in acid mine water. Hydrogeology & Engineering Geology, 52(5): 1−10. DOI：10.16030/j.cnki.issn.1000-3665.202505013.

Zhang Z, Zhu M, Li J, et al. 2019. Effect of heat treatment on the combustion characteristics of a lignite. Journal of Energy Resources Technology, 141(7): 070705. DOI：10.1115/1.4042823.

Zhao Y, Naeth MA. 2024. Cd (II) and Zn (II) adsorption on lignite-derived humic substances and cattle manure biochar. CLEAN–Soil, Air, Water, 52(8): 2400226. DOI：10.1002/clen.202400226.